Korea Institute of Science and Technology KIST

리튬공기전지 소재 기술 개발 현황

Recent Development of Advanced Materials For Li-Air Batteries

1. 공기극 (cathode)

정 훈 기

한국과학기술연구원

hungi@kist.re.kr

공기극 – Carbon electrode

Korea Institute of Science and Technology

Pencil-drawing on a ceramic state electrolyte

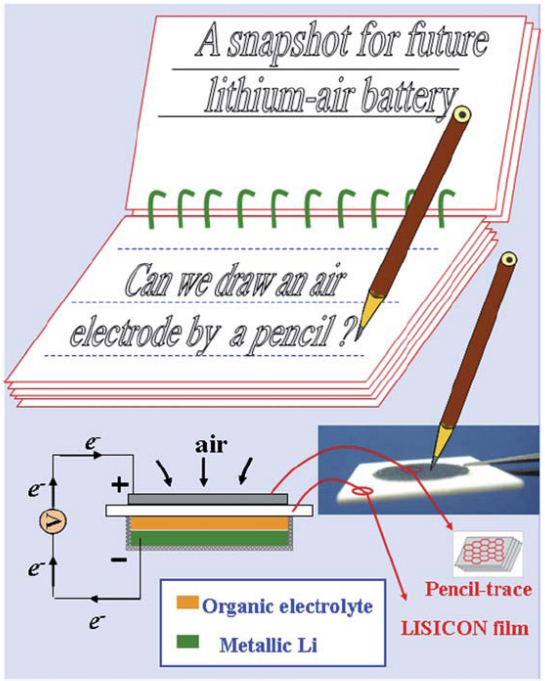

Fig. 1 A schematic representation of the pencil-drawing process, and the structure of the proposed lithium–air battery.

Y. Wang and H. Zhou, *Energy Environ. Sci.*, 2011, 4, 1704

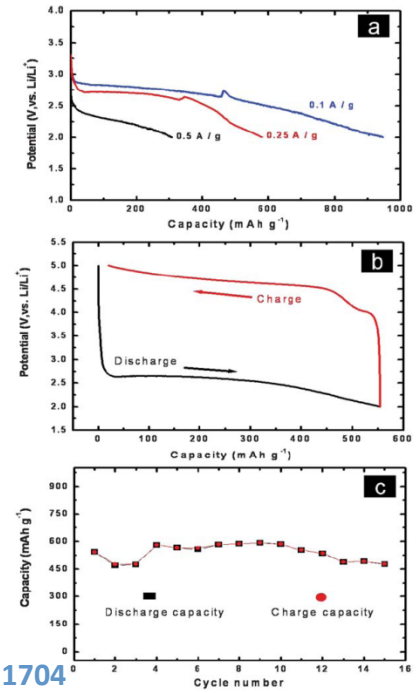

Fig. 3 The electrochemical performance of the proposed lithium–air battery. (a) Discharge curves at different current densities. (b) A charge–discharge curve tested with a current density of 0.25 A g^{-1}. (c) Cycling performance tested with a current of 0.25 A g^{-1}.

Hierarchically Porous Graphene

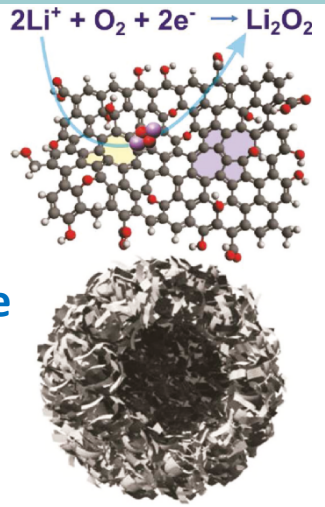

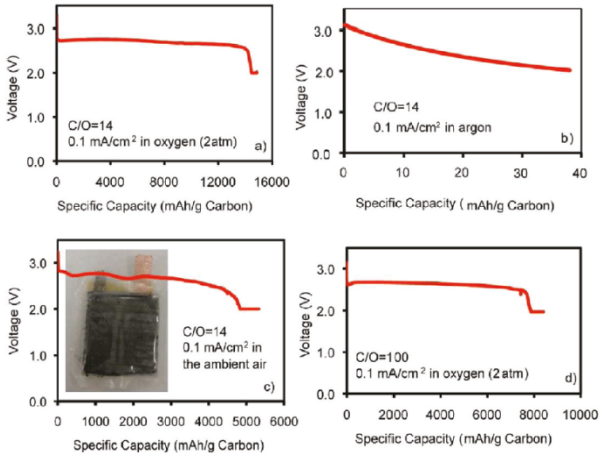

Figure 3. Electrochemical performances of Li−air batteries using FGS as the air electrodes. (a) The discharge curve of a Li−O_2 cell using FGS(C/O = 14) as the air electrode (P_{O_2} = 2 atm). (b) The same Li−O_2 cell as in (a) but tested in the pure argon atmosphere. (c) Discharge curve of a pouch-type Li−air cell made from FGS (C/O = 14) operated in ambient environment (P_{O_2} = 0.21 atm, relative humidity = 20%). The inset shows the prototype of the pouch cell. (d) The discharge curve of a Li−O_2 cell using FGS (C/O = 100) as the air electrode (P_{O_2} = 2 atm).

J.-G. Zhang et al., Nano Letters, 2011, 11, 5071

공기극 – Carbon electrode

Korea Institute of Science and Technology

Carbon is relatively stable below 3.5 V on discharge or charge (hydrophobic) but is unstable on charging above 3.5 V (in the presence of Li_2O_2), oxidatively decomposing to form Li_2CO_3.

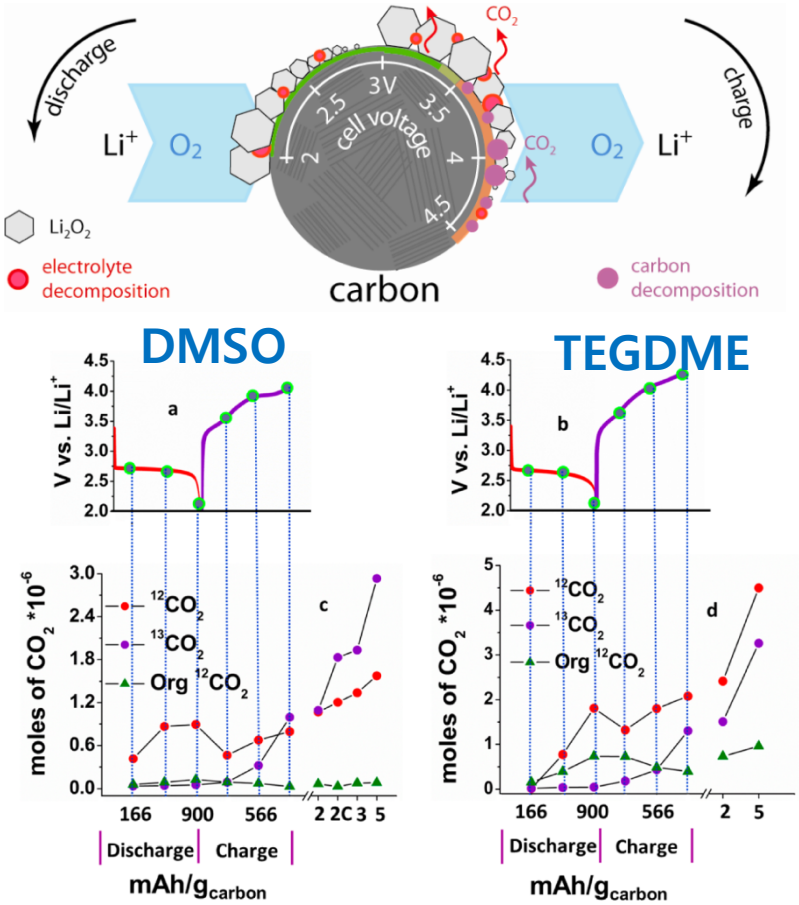

Figure 1. (a,b) Discharge–charge curves on the first cycle for DMSO- and tetraglyme-based electrolytes, respectively, at a carbon cathode; rate: 70 mA/g_{carbon}. (c,d) Moles of CO_2 evolved from the carbon cathodes, removed from the cells at the states of discharge and charge indicated by the green dots in (a,b), and then treated with acid to decompose $Li_2{}^{12}CO_3$ and $Li_2{}^{13}CO_3$ and Fenton's reagent to decompose the lithium carboxylates. The values (166 etc.) on the *x*-axis do not represent a scale but indicate the states-of-charge at which the cathodes were sampled. The numbers 2, 3, and 5 in (c) and 2 and 5 in (d) correspond to the electrodes analyzed at the end of discharge on those cycles, and the number 2C in (c) corresponds to the analysis of the carbon electrode at the end of the second charge.

P. G. Bruce *et al.*, *J. Am. Chem. Soc.* 135 (2013) 494–500

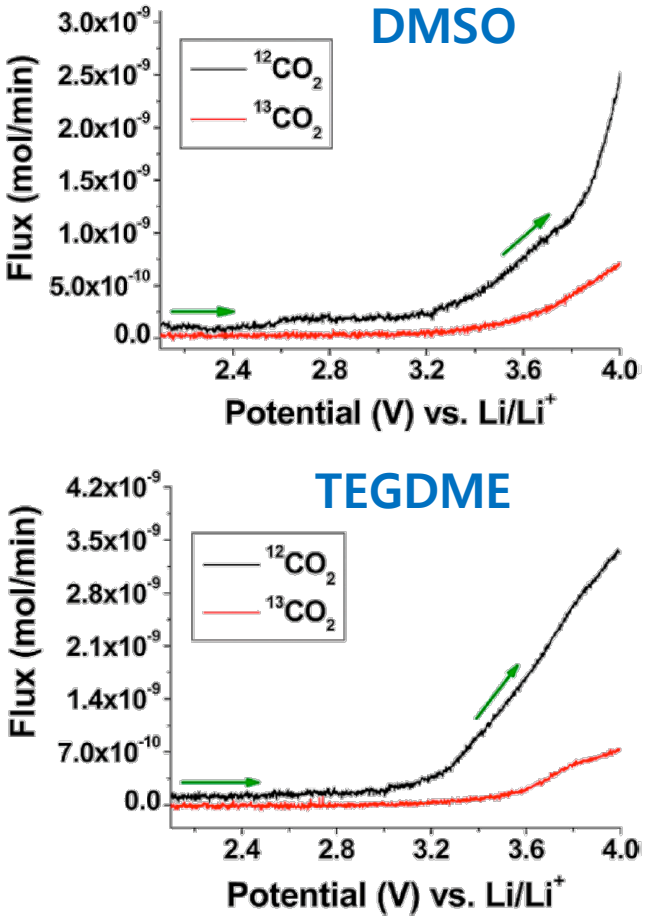

Figure 3. In situ DEMS data for CO_2 evolution from decomposition of products formed from the electrolyte ($^{12}CO_2$) and the carbon cathode ($^{13}CO_2$) in (a) DMSO- and (b) tetraglyme-based electrolyte; for the first charge after discharge to 2 V. Charging is carried out in an Ar:O_2 gas mixture (5:95 v/v).

공기극 – MnO_2 catalyst

Korea Institute of Science and Technology

α-MnO_2 Nanowires

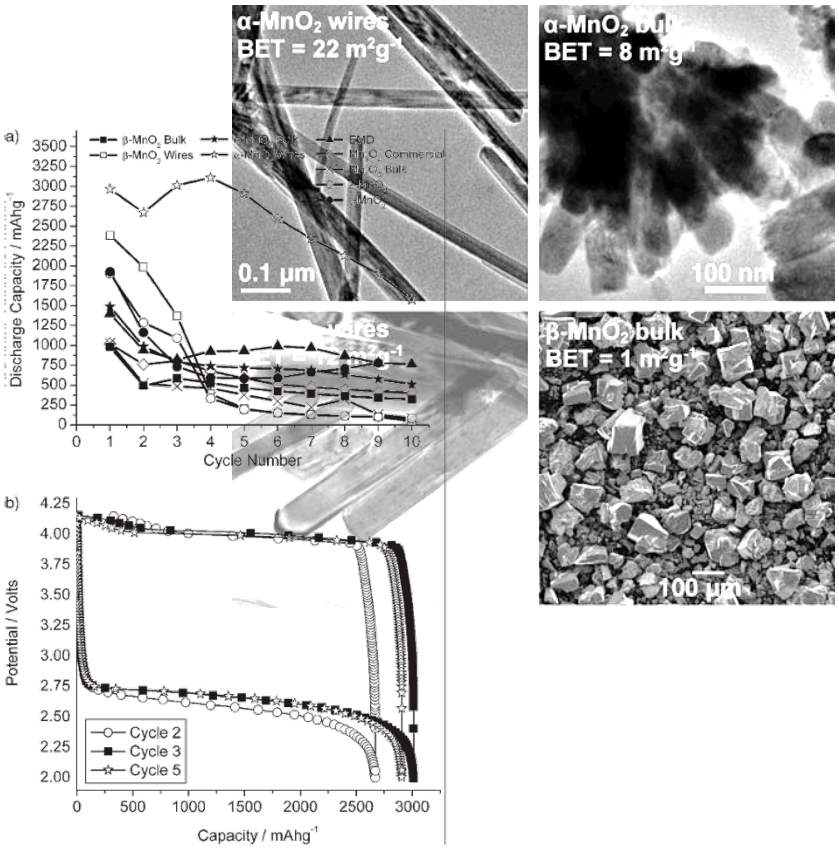

Figure 2. a) Variation of discharge capacity with cycle number for several porous electrodes containing manganese oxides as catalysts: α-MnO_2 in bulk and nanowire form, β-MnO_2 in bulk and nanowire form, γ-MnO_2, λ-MnO_2, Mn_2O_3, and Mn_3O_4. EMD is included herein for comparison but was reported previously.[8] Cycling was carried out at a rate of 70 mAg^{-1} in 1 atm of O_2. Capacities are per gram of carbon in the electrode. Lower cutoff potential 2 V. b) Variation of potential with state of charge for the porous electrode containing α-MnO_2 nanowires reported in Figure 2a, cycled at a rate of 70 mAg^{-1} between 2 and 4.15 V.

P.G. Bruce *et al.*, Angew. Chem. Int. Ed. 2008, 47, 4521 –4524

α-MnO_2/ramsdellite-MnO_2 electrode

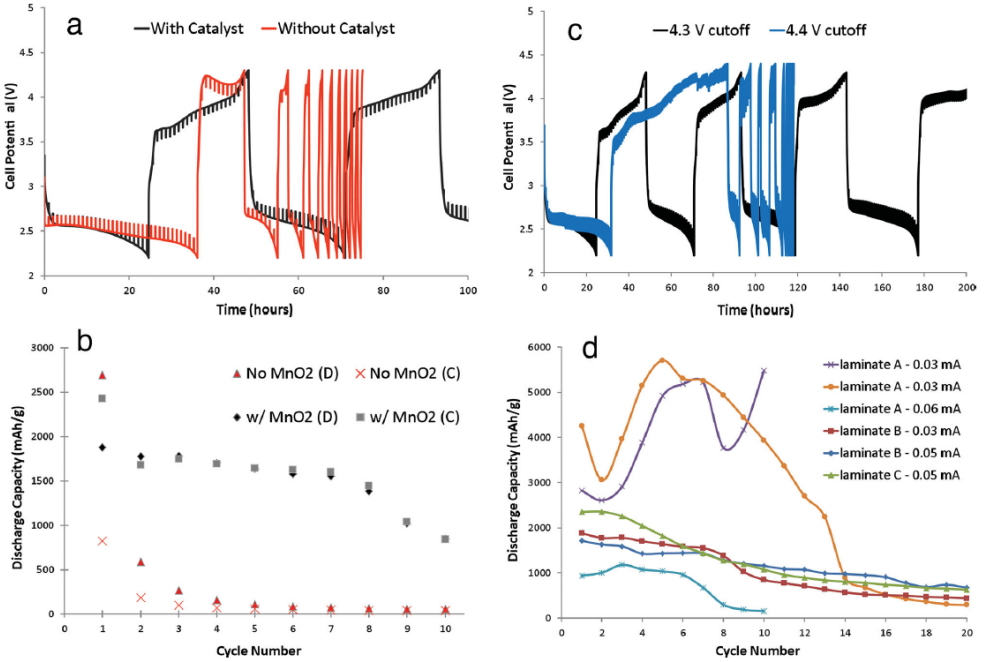

Figure 4. Electrochemical data of Li/O_2 cells, (a) with and without a α-MnO_2/R-MnO_2 electrode/electrocatalyst; (b) cycling data with and without a α-MnO_2/R-MnO_2 electrode/electrocatalyst (C = charge, D = discharge); (c) with a α-MnO_2/R-MnO_2 electrode/electrocatalyst to upper charging voltages of 4.3 V and 4.4 V; and (d) capacity vs. cycle number for three separately made laminates (A, B, and C) each with the α-MnO_2/R-MnO_2 electrode/electrocatalyst at various current rates.

L. Trahey *et al.*, Adv. Energy Mater. 3 (2013) 75-84

공기극 – Pt based catalyst

Korea Institute of Science and Technology

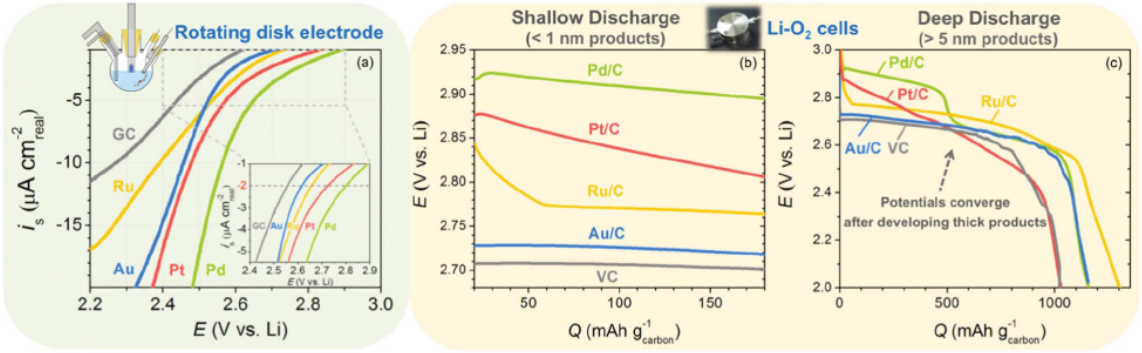

Fig. 10 (a) Specific ORR net current densities, i_s, on GC, Pd, Pt, Ru and Au in O_2-saturated 0.1 M $LiClO_4$ DME at 100 rpm and 20 mV s^{-1}. Initial (b) and full (c) discharge profiles of Pd/C, Pt/C, Ru/C, Au/C and Vulcan carbon (VC) in 0.1 M $LiClO_4$ in DME at 100 mA g_C^{-1} in Li–O_2 cells. The average estimated thickness of discharge products was calculated from discharge capacities assuming uniform distribution of Li_2O_2 on the electrode surfaces. Adapted from ref. 58.

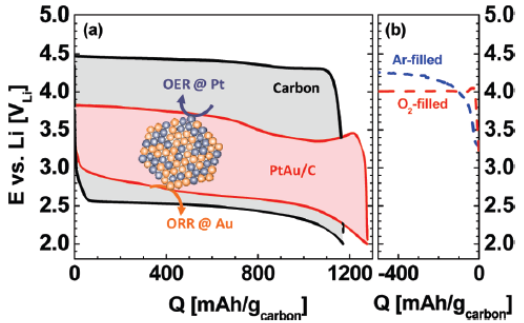

Figure 2. (a) Li−O_2 cell discharge/charge profiles of carbon (black, 85 mA/g_{carbon}) and PtAu/C (red, 100 mA/g_{carbon}) in the third cycle at 0.04 mA/$cm^2_{electrode}$. (b) Background measurement during charging at 100 mA/g_{carbon} of Ar- and O_2-filled cells (charging first) for PtAu/C.

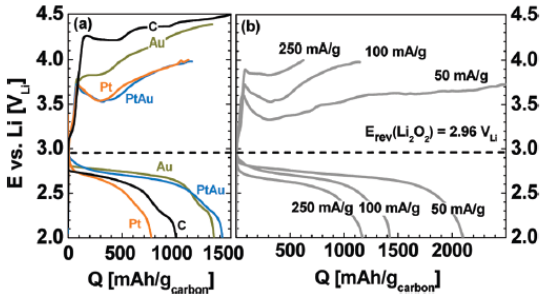

Figure 3. (a) Li−O_2 cell first discharge/charge profiles of carbon at 85 mA/g_{carbon} and of Au/C, Pt/C, and PtAu/C at 100 mA/g_{carbon}. (b) Li−O_2 cell discharge/charge profiles (first cycle) of PtAu/C at 50, 100, and 250 mA/g_{carbon}. (See SI, Figure S5, for background measurements.)

Y. Shao-Horn et al., J. Am. Chem. Soc., 2011, 133, 19048–19051.
Y. Shao-Horn et al., J. Am. Chem. Soc., 2010, 132, 12170–12171

Pt catalyzes electrolyte decomposition in the presence of O_2.

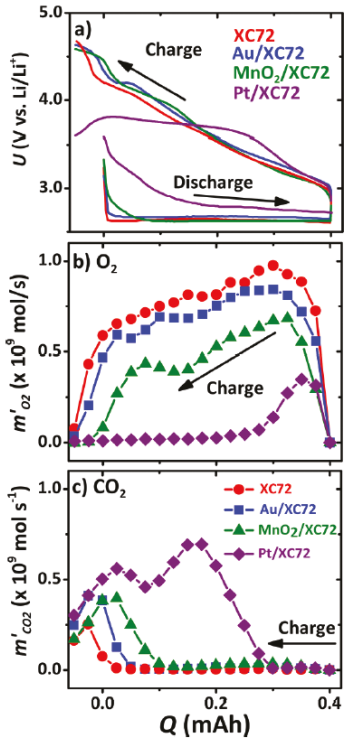

Figure 2. Gas evolution from cells employing DME. (a) Discharge−charge voltage curves, and corresponding O_2 (b) and CO_2 (c) evolution during charging of cells using various cathode catalysts.

Bryan D. McCloskey et al., J. Am. Chem. Soc. 2011, 133, 18038–18041

공기극 – Ru based catalyst

Korea Institute of Science and Technology

Ru and RuO_2 based catalyst

H.-G. Jung et al., ACS Nano, 2013, 7, 3532-3539

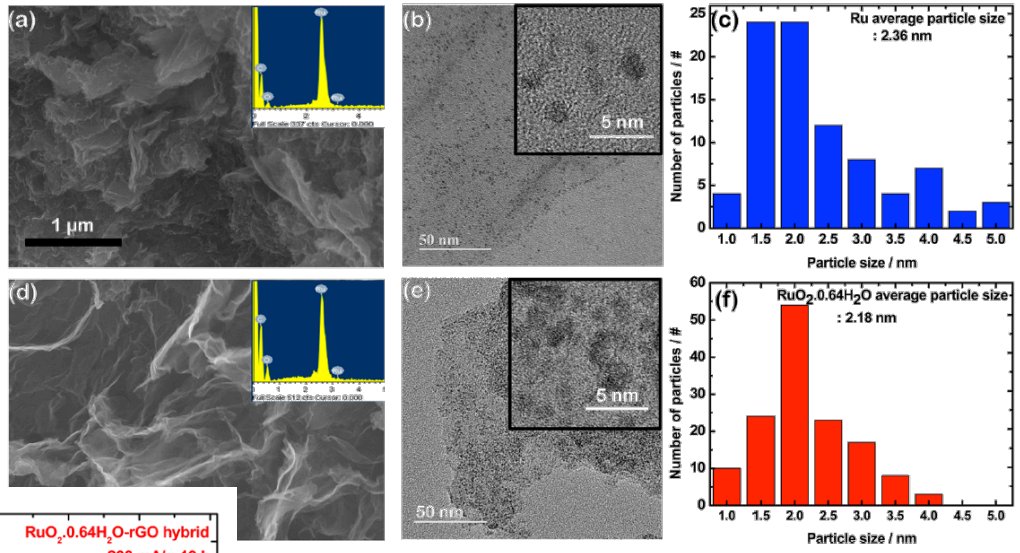

alysis of Ru-rGO and $RuO_2 \cdot 0.64H_2O$-rGO hybrids: (a) SEM image of porous Ru-rGO hybrid; (inset) (b) TEM images of Ru-rGO hybrid (inset: HRTEM image); (c) particle size distribution of Ru-rGO ous $RuO_2 \cdot 0.64H_2O$-rGO hybrid; (inset) SEM-EDX of $RuO_2 \cdot 0.64H_2O$-rGO hybrid; (e) TEM images of inset: HRTEM); and (f) particle size distribution of $RuO_2 \cdot 0.64H_2O$-rGO hybrid.

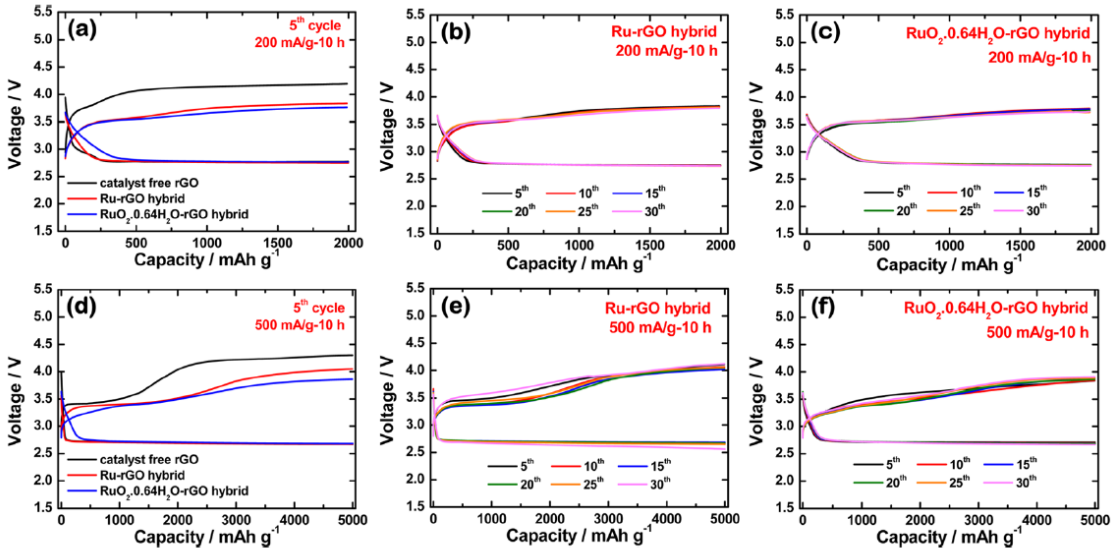

Figure 2. Discharge–charge cycles of Li-air cells using rGO, Ru-rGO hybrid, and $RuO_2 \cdot 0.64H_2O$-rGO hybrid under various specific capacity limits. (a–c) Current = 200 mA g^{-1}; time = 10 h; cycling capacity = 2000 mAh g^{-1}; voltage profiles of (a) fifth cycle and following cycles of (b) Ru-rGO hybrid and (c) $RuO_2 \cdot 0.64H_2O$-rGO hybrid. (d–f) Current = 500 mA g^{-1}; time = 10 h; cycling capacity = 5000 mAh g^{-1}; voltage profiles of (d) fifth cycle and following cycles of (e) Ru-rGO hybrid and (f) $RuO_2 \cdot 0.64H_2O$-rGO hybrid. The capacity was normalized by the total weight of oxygen electrodes (rGO or rGO + catalyst).

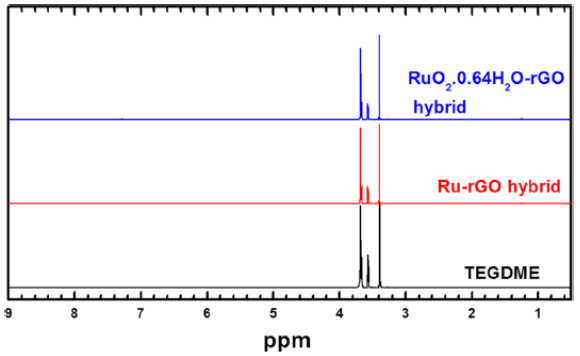

Figure 3. Comparison of ^1H NMR spectra obtained for a TEGDME electrolyte of Li-air cells using rGO, Ru-rGO hybrid, and $RuO_2 \cdot 0.64H_2O$-rGO hybrid after cycling test (capacity = 5000 mAh g^{-1}).

공기극 – Other Catalyst

Korea Institute of Science and Technology

Co_3O_4 nanocrystals on graphene

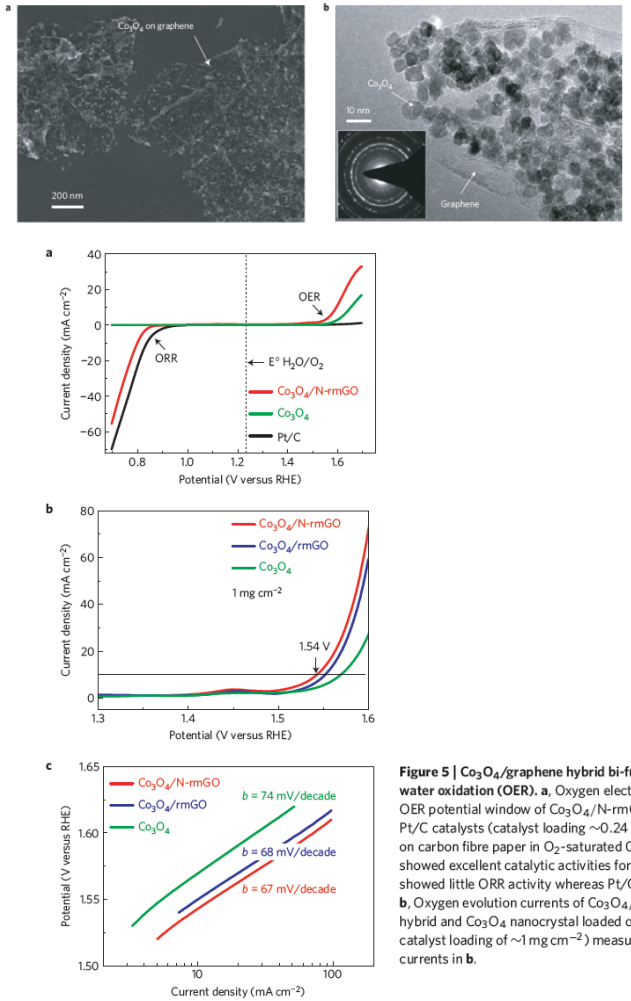

Figure 5 | Co_3O_4/graphene hybrid bi-functional catalyst for ORR and water oxidation (OER). a, Oxygen electrode activities within the ORR and OER potential window of Co_3O_4/N-rmGO hybrid, Co_3O_4 nanocrystal and Pt/C catalysts (catalyst loading ~0.24 mg cm^{-2} for all samples) dispersed on carbon fibre paper in O_2-saturated 0.1 M KOH. Co_3O_4/N-rmGO hybrid showed excellent catalytic activities for both ORR and OER. Free Co_3O_4 showed little ORR activity whereas Pt/C showed little OER activity. **b**, Oxygen evolution currents of Co_3O_4/N-rmGO hybrid, Co_3O_4/rmGO hybrid and Co_3O_4 nanocrystal loaded onto Ni foam (to reach a high catalyst loading of ~1 mg cm^{-2}) measured in 1 M KOH. **c**, Tafel plots of OER currents in **b**.

Hongjie Dai et al., Nat. Mater., 2011, 10, 780-786

Carbon supported TiN nanoparticles

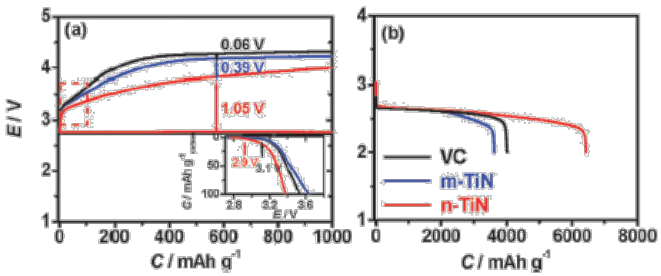

Fig. 3 (a) Discharge–recharge curves of VC, m-TiN/VC, and n-TiN/VC as cathode catalysts of Li–O_2 batteries and an enlarged section highlighted (inset) at 50 mA g_{carbon}^{-1} and (b) their discharge curves at 500 mA g_{carbon}^{-1}.

H. Zhou et al., Chem. Commun., 2013, 49, 1175--1177

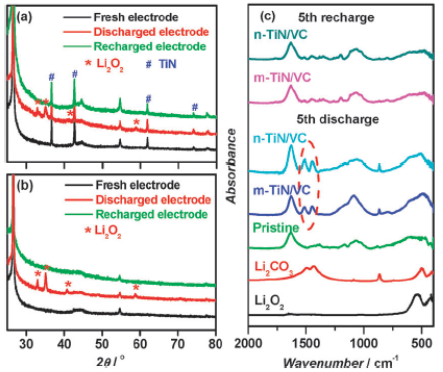

Fig. 4 XRD patterns of fresh, discharged, and recharged electrodes based on m-TiN/VC (a) and n-TiN/VC (b), and FT-IR spectra at the 5th discharge and recharge (c).

Oxide based catalyst

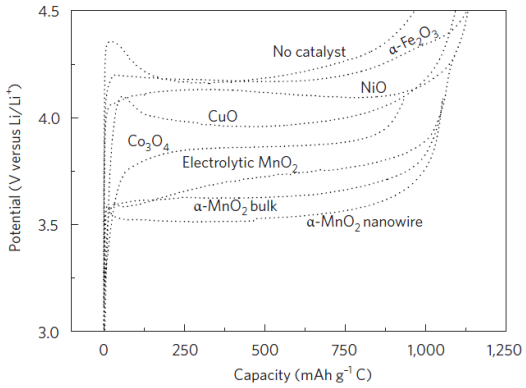

Figure 4 | First galvanostatic charge, i = 70 mA g^{-1} C (that is, Li_2O_2 oxidation) for various catalyst-containing Li-O_2 cells in this study[77]. Figure adapted with permission from ref. 77, © 2010 ECS.

P.G. Bruce et al., Electrochem. Solid St. 13, A180–A183 (2010)

공기극 – Nanoporous gold (NPG)

Korea Institute of Science and Technology

NPG electrode foils (dealloying white gold leaf)

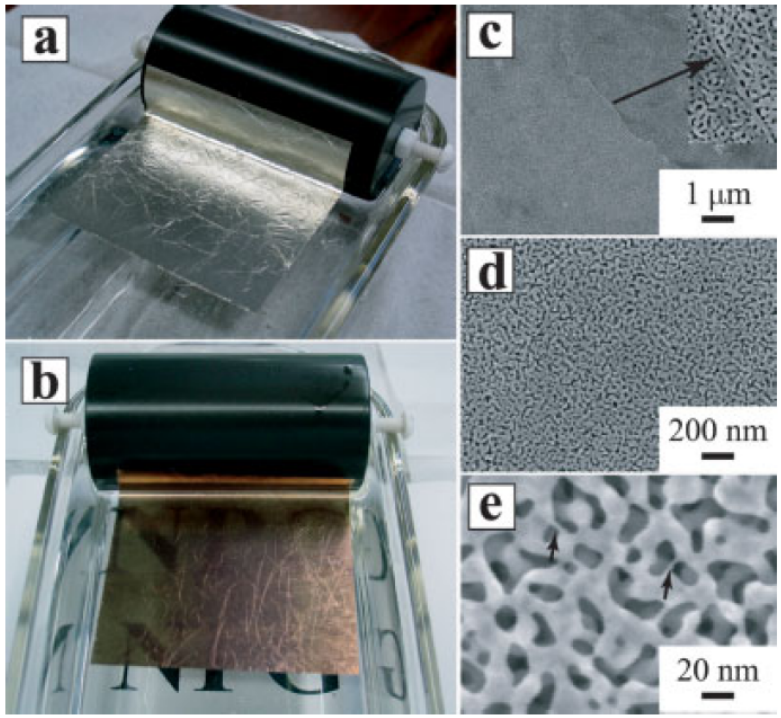

Figure 1. a,b) Optical and c–e) SEM images of white-gold leaf before and after dealloying in nitric acid for 15 min. The inset image in (c) shows a region where a solid grain boundary is located. Very thin gold ligaments with diameters smaller than 2 nm are often observed; examples are marked with arrows in (e).

Y. Ding et al., Adv. Mater. 16, 1897 (2004).

Using Freestanding thin film of NPG (Pore : 30-50 nm)

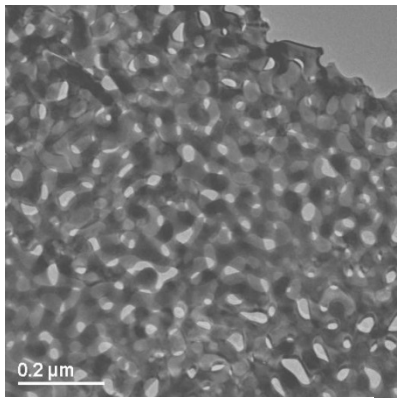

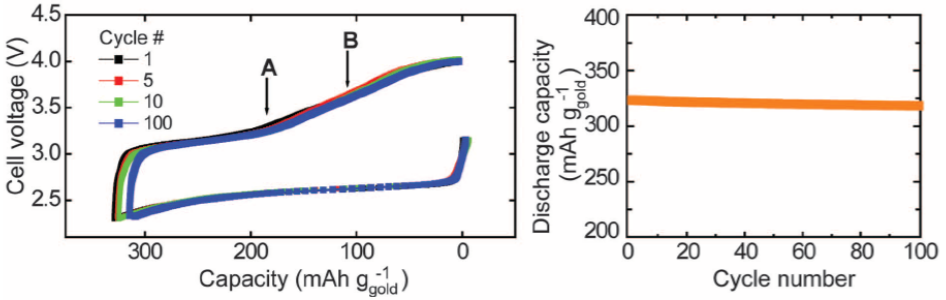

Fig. 1. Charge/discharge curves (**left**) and cycling profile (**right**) for a Li-O_2 cell with a 0.1 M $LiClO_4$-DMSO electrolyte and a NPG cathode, at a current density of 500 mAg^{-1} (based on the mass of Au). Because the capacities are given per gram of Au, which is ~10-fold heavier (more dense) than carbon, 300 $mAhg^{-1}$ (based on the mass of Au) would, for the same porous electrode but formed from carbon, correspond to ~3000 $mAhg^{-1}$ (based on the mass of carbon). FTIR spectra collected upon charging at points A and B are shown in fig. S7.

P. G. Bruce *et al.*, *Science*,337 (2012) 563-566

리튬공기전지 소재 기술 개발 현황

Recent Development of Advanced Materials For Li-Air Batteries

2. 음 극 (Anode)

리튬금속 음극

Highest theoretical capacity of 3,862 mAh/g (compared to graphitic carbon capacity of 370 mAh/g)

- **Free from lithium intercalated cathode**

Issues

Dendrite formation resulting in loss of lithium, possibly a safety hazard.
Solvent reduction resulting in loss of lithium and electrolyte.

Approaches

Decouple lithium metal from cathode chemistry with an interphase layer stable with lithium, having good ionic conductivity and a low interfacial impedance.

- **Block copolymers (Seeo)**
- **Multiple polymer/ceramic layers (Sion Power)**
- **Single Ion Conducting Ceramic (PolyPlus)**

Pre lithiated Si electrode

Korea Institute of Science and Technology

The hard carbon sphere-sulfur composite cathode

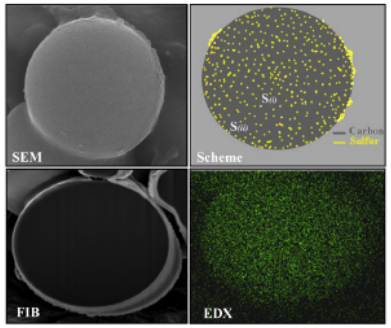

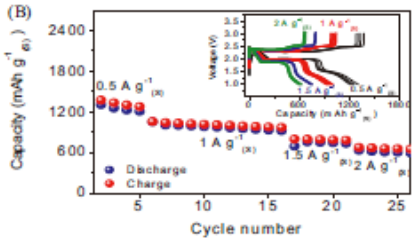

Y-.K. Sun, *Journal of Power Sources*, 2012 (202) 308-313

Pre Lithiated Si-C composite anode

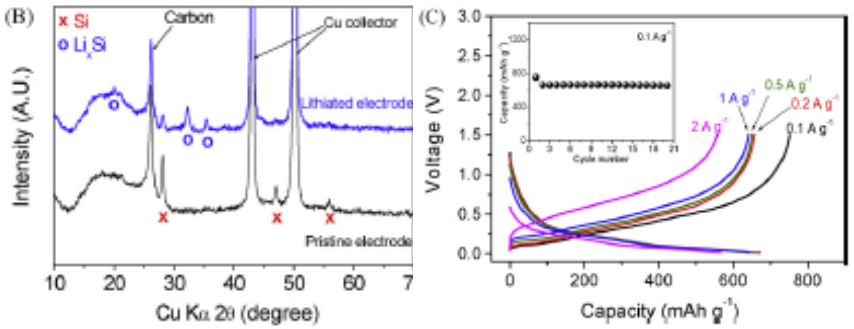

Y-.K. Sun, *Journal of Power Sources*, 2012 (202) 308-313

Li-Si-C/ TEGDME electrolyte/ HCS-S
Lithium-Silicon-Sulfur battery

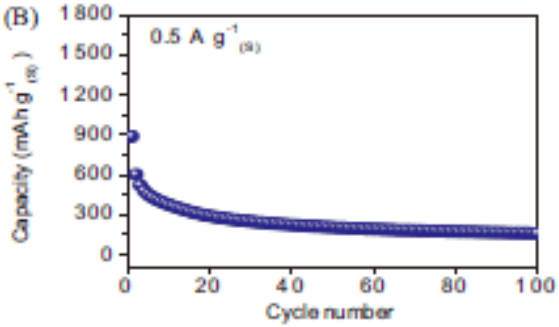

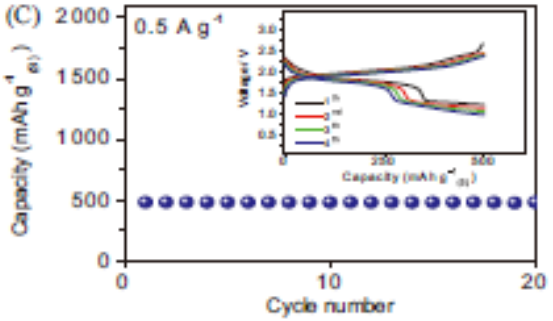

Y-.K. Sun, *Journal of Power Sources*, 2012 (202) 308-313

리튬금속을 사용하지 않은 리튬공기전지

Korea Institute of Science and Technology

Li-Metal free Air battery

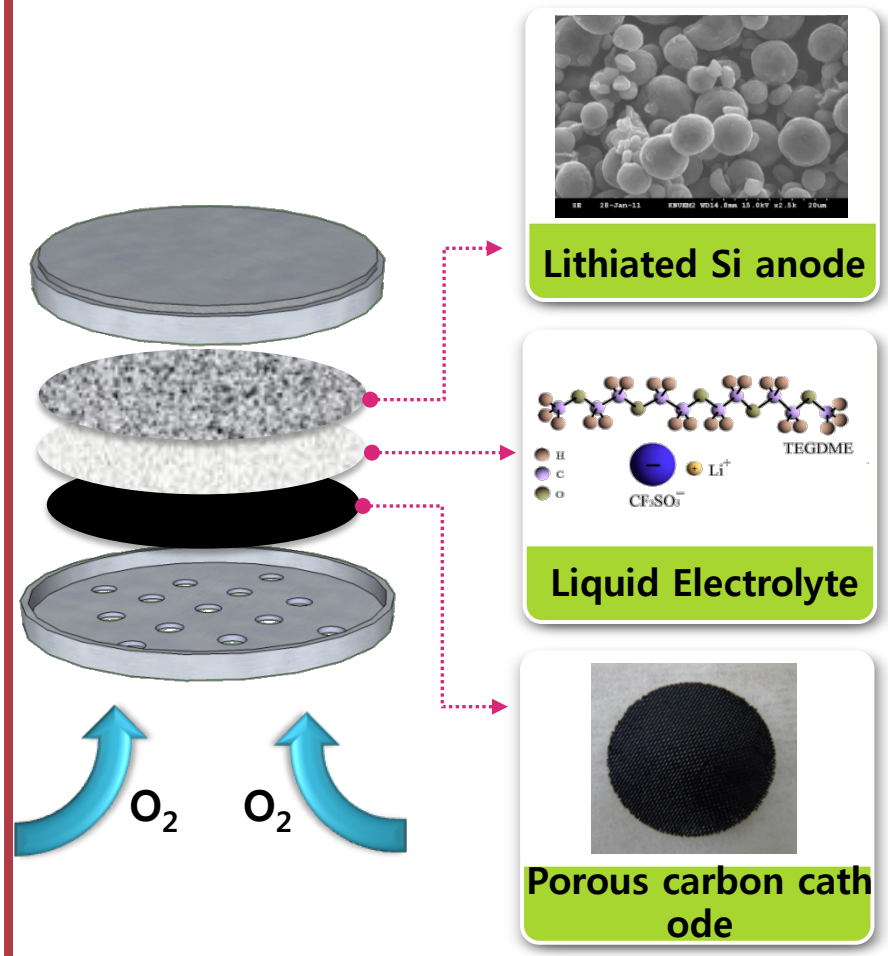

Performance of Li-air cell

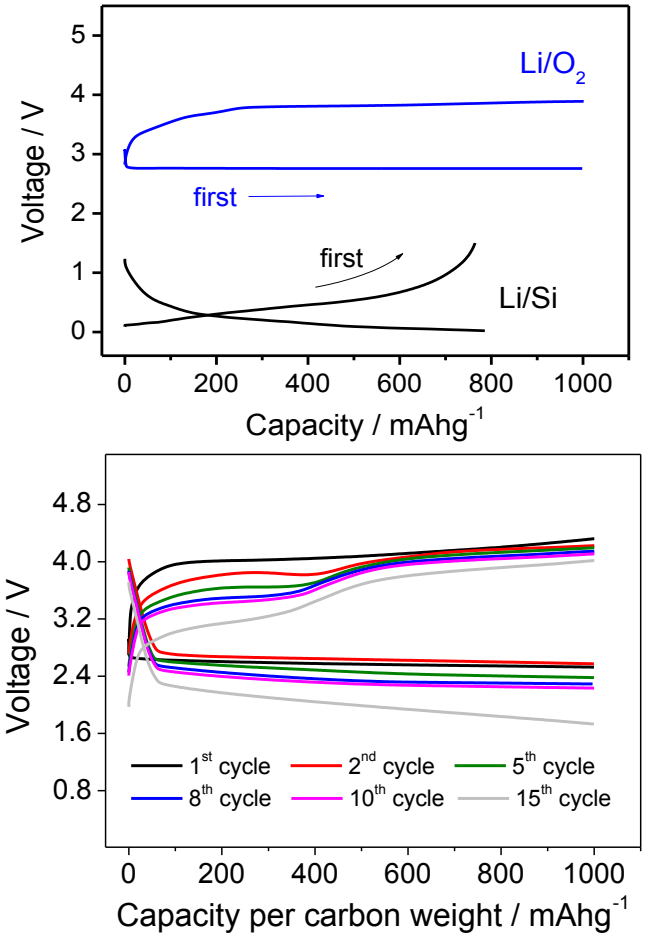

H.-G. Jung et al. ***Nano Letters*** **12**, *5775-5779* (2012).